Journal of Applied Polymer Science

Dynamic Properties of Star-Shaped, Solution-Polymerized Styrene–Butadiene Rubber and Its Cocoagulated Rubber-Filled with Silica/Carbon Black

Xiao Liu,[1] Suhe Zhao,[2,3] Yong Yang,[2] Xingying Zhang,[2,3] Youping Wu[2,3]

[1]College of Materials Science and Engineering, Beijing University of Technology, Beijing 100124, China

[2]Key Laboratory of Beijing City on the Preparation and Processing of Novel Polymer Materials, Beijing University of Chemical Technology, Beijing 100029, China

[3]Key Laboratory for Nanomaterials, Ministry of Education, Beijing University of Chemical Technology, Beijing 100029, China

Correspondence to: S. Zhao (E-mail: zhaosh@mail.buct.edu.cn)

ABSTRACT: The dynamic properties, including the dynamic mechanical properties, flex fatigue properties, dynamic compression properties, and rolling loss properties, of star-shaped solution-polymerized styrene–butadiene rubber (SSBR) and organically modified nanosilica powder/star-shaped styrene–butadiene rubber cocoagulated rubber (N-SSBR), both filled with silica/carbon black (CB), were studied. N-SSBR was characterized by ^{1}H-NMR, gel permeation chromatography, energy dispersive spectrometry, and transmission electron microscopy. The results show that the silica particles were homogeneously dispersed in the N-SSBR matrix. In addition, the N-SSBR/SiO_2/CB–rubber compounds' high bound rubber contents implied good filler–polymer interactions. Compared with SSBR filled with silica/CB, the N-SSBR filled with these fillers exhibited better flex fatigue resistance and a lower Payne effect, internal friction loss, compression permanent set, compression heat buildup, and power loss. The nanocomposites with excellent flex fatigue resistance showed several characteristics of branched, thick, rough, homogeneously distributed cross-sectional cracks, tortuous flex crack paths, few stress concentration points, and obscure interfaces with the matrix. Accordingly, N-SSBR would be an ideal matrix for applications in the tread of green tires. © 2014 Wiley Periodicals, Inc. J. Appl. Polym. Sci. **2014**, *131*, 40348.

KEYWORDS: applications; blends; properties and characterization; rubber; surfaces and interfaces

Received 18 September 2013; accepted 27 December 2013

DOI: 10.1002/app.40348

INTRODUCTION

Since the 1990s, with the increase in environmental awareness, there is an increasing need for a reduction of car fuel consumption and exhaust emission. Nearly 6.6% of the fuel consumption of cars comes from the energy consumption of tires. Furthermore, 49% of the tire's total rolling resistance is from treads. The other sources are sidewalls (14%), carcasses (11%), beads (11%), belts (8%), and other parts (7%). This dynamic and periodic deformation of tires in the vehicle driving process leads to hysteresis behavior and heat generation, and this contributes to the tire's rolling resistance. Therefore, a decrease in the heat buildup of tire tread materials is an effective method for reducing the tire's rolling resistance.

Vulcanizates reinforced by silica exhibits many advantages, including good dynamic properties. Thus, silica has played a more and more important role in preparing green tire tread materials.[1–5] With excellent reinforcement and abrasion resistance, carbon black (CB) is also one kind of indispensable filler for the preparation of tire tread materials.[6–8] Furthermore, star-shaped solution-polymerized styrene–butadiene rubber (SSBR) with end groups coupled by $SnCl_4$ has many characteristics, including a low internal friction loss, few free macromolecular terminals, and good wet traction. Therefore, tire tread materials mainly prepared by SSBR show a high wet-skid resistance and relatively good dynamic properties, including a low heat buildup and a low rolling resistance. As a matrix, SSBR has been widely used as a tire tread material for modern cars in recent years. Accordingly, research into the dynamic properties of SSBR filled with silica and CB will further widen its applications in the tire industry to achieve energy saving and to prevent exhaust pollution.

The technology of nanocomposites between the SSBR matrix and nanofillers is a problem to be solved for researchers. Silica has a considerably large specific surface area and a strong self-aggregation, and thus, the key to nanocomposite technology is the achievement of a good dispersion of inorganic particles in

the polymer matrix with nanosize and strong interfacial interaction between inorganic particles and organic macromolecules. In the general solution, silica particles are organically modified by a silane coupling agent and then mixed with the polymer matrix.[9,10] The affinity between the modified silica and rubber macromolecules is partially improved, but it is still difficult to obtain an SSBR/SiO_2 composite with a nanodispersed filler. Star-shaped SSBR used as a tread material in high-performance tires is produced by solution polymerization and, thus, is in a solution state. When the organically modified silica is mixed in solvent and is then entirely added to the polymer solution, the nanocomposite also can be obtained through the process of homogeneous stirring, the removal of solvent, and cocoagulation. However, there have been few studies on this.

In a previous article,[11] we described the preparation of SiO_2/CB-filled vulcanizates with SSBR and nanosilica powder/star-shaped styrene–butadiene rubber cocoagulated rubber (N-SSBR) as polymer matrices and investigated their morphological structures and many mechanical properties. In addition, the effects of the filler ratio and matrix on these properties were studied in detail. As pointed out in that article, nanocomposites with some excellent performances were obtained with N-SSBR as the matrix. Because the targeted application of the nanocomposites is in tire tread materials, it is necessary to investigate their dynamic properties. Up to this point, there have been only a few studies on the dynamic properties of SSBR filled with silica.[12,13] Furthermore, reports of silica/cocoagulated rubber and SSBR filled with both silica and CB at different filler ratios and the investigation of their dynamic properties, both detailed and overall, have not been mentioned.

In this study, the dynamic mechanical properties, flex fatigue properties, dynamic compression properties, and rolling loss of star-shaped SSBR and N-SSBR filled with both silica and CB at different filler ratios were studied. These properties share one common feature: that the testing was carried out in a dynamic process but a not static process. The experimental data were analyzed through filler–polymer interaction, filler dispersion, and interfacial bonding. In addition, the effects of the use of N-SSBR on the dynamic properties and the variations of filler–filler and polymer–filler interactions in the dynamic process were also investigated. Because the properties experimentally measured in this study have also been emphatically investigated in the tire industry, our research work will provide significant guidance for the preparation of green tire tread materials.

EXPERIMENTAL

Materials and Compounding

Star-shaped SSBR was supplied by the Synthetic Rubber Plant of Yanshan Petrochemical Co., Ltd. (Beijing, China). N-SSBR was prepared by the addition of 7 parts per hundred of rubber (phr) silica powder to the star-shaped SSBR solution and then coagulation. The precipitated silica (Tixosil 383), with an average particle diameter of 20–40 nm and a specific surface area of 100–200m^2/g, was provided by Rhodia Co., Ltd. (Qingdao, China). CB (N234) came from Tianjin Dolphin Carbon Black Co., Ltd. (Tianjin, China). The silane coupling agent, [3-(2-aminoethyl) aminopropyl] trimethoxysilane, was produced by Beijing Shenda Fine Chemical Co., Ltd. (Beijing, China). The other rubber additives, including zinc oxide, stearic acid, and sulfur, were commercial grade.

Formulation

A typical composition of the prepared SSBR/SiO_2/CB nanocomposite is listed in Table I. The N-SSBR/SiO_2/CB nanocomposite had the same composition, except for the matrix, which was N-SSBR.

The amounts of silica and CB were varied to prepare compounds with different ratios of hybrid filler, and the total amount of filler was kept constant at 50 phr in each composite. The [3-(2-aminoethyl)aminopropyl] trimethoxysilane amount was 7% of the mass of nanosilica powder.

The samples were identified as follows (the C series employed SSBR as the matrix, and the N series employed N-SSBR as the matrix):

SSBR was filled with various SiO_2/CB ratios. The samples with ratios of 50/0, 30/20, 20/30, and 10/40 were named C1, C2, C3, and C4, respectively. N-SSBR filled with ratios of 50/0, 30/20, 20/30, and 10/40 of SiO_2/CB were named N1, N2, N3, and N4, respectively. Additionally, the previous silica loadings contained the amounts of silica in the N-SSBR.

Preparation of the Organically Modified Silica and N-SSBR

Silica powder was added to an ethanol solution of the silane coupling agent to be a mixture at a concentration of 0.01–0.1 g/mL, and then stirred at 300rpm for 6 h to ensure the homogeneous dispersion, followed by placing overnight at room temperature. After the ethanol vaporized completely, the silica powder-coated with silane coupling agent was placed in an air-circulating oven at 80°C for an hour.

The organically modified silica powder obtained as described previously was dispersed in cyclohexane to prepare a silica–cyclohexane solution with a concentration of 0.01–0.1 g/mL. After strong stirring for a moment, the mixture was added to the SSBR solution and then stirred again at 200rpm for 6 h.

Table I. Compounding Formulation

Ingredient	Loading (phr)
Rubber (SSBR)	100
Silica (Tixosil 383)	Variable[a]
CB (N234)	Variable[a]
Zinc oxide	4
Stearic acid	1
Antioxidant[b]	1.5
Accelerator CZ[c]	1.2
Accelerator TT[d]	0.1
Liquid coumarone[e]	5
Sulfur	1.8

[a] The overall filler content was kept at 50 phr.
[b] Polymerized 2,2,4-trimethyl-1,2-dihydroquinoline.
[c] CZ, *N*-cyclohexyl-2-benzothiazole sulfenamide.
[d] TT, tetramethyl thiuram disulfide.
[e] Added only to the composites containing CB.

Then, the SSBR/SiO_2 cocoagulated rubber, that is, N-SSBR, could be obtained by the removal of the solvent.

Instruments and Techniques of Mixing and Vulcanization

All of the ingredients were mixed with rubber in a 6-in. internal mixer (Shanghai Rubber Machinery Works, Shanghai, China) at a set temperature of 50°C with a front roller speed of 8.95 m/min and a roller speed ratio of 1:1.35. The total mixing time in the internal mixer was about 15 min. After it was discharged, the compound was sheeted off and was then placed for 24 h before vulcanization.

Curing characteristics, including the scorch time, curing time (t_{90}), and minimum torque of the rubber compound, were determined at 150°C with a P3555B2 oscillating disk rheometer (Beijing Huanfeng Chemical Machinery Trial Plant, Beijing, China). About 6.5 g of the rubber compound was used for each test, and a 1° arc oscillating angle was applied. The t_{90} used for sample vulcanization was the time at which the rheometer torque increased to 90% of the total torque change on the curing curve.

An XLB-D350 × 350 plate vulcanization machine (Huzhou Dongfang Machinery Co., Ltd., Zhejiang, China) was used to prepare the vulcanizates, and the curing conditions were 150°C at t_{90}. The hydraulic pressure was 15 MPa, and the vulcanizates had a thickness of about 2 mm.

Characterization

The number-average molecular weight (M_n), weight-average molecular weight (M_w), and polydispersity index (M_w/M_n) of N-SSBR were measured with a Waters150-C gel permeation chromatograph (Waters Corp.) with three Waters Styragel columns (pore sizes = 10^2, 10^3, and 10^4 Å, respectively) in series calibrated by a narrow polystyrene standard with molecular weights ranging from 2.2×10^3 to 5.15×10^5 g/mol. Tetrahydrofuran was used as the eluent at a flow rate of 1.0 mL/min at 40°C.

The characteristic groups of N-SSBR were tested by ^{1}H-NMR measurements carried out on a Bruker AV600 high-resolution NMR spectrometer (Bruker Corp., Bremen, Germany) with a frequency of 600 MHz at room temperature (25°C). The polymer sample was dissolved in $CDCl_3$ in a 5-mm NMR tube. Chemical shifts are reported in parts per million and were referenced to tetramethylsilane as an internal standard and calculated with the residual isotopic impurities of the deuterated solvents.

The elemental distributions on the surfaces of the sample residues were analyzed by a Hitachi S-4300 field emission scanning electron microscope equipped with a Genesis-60 energy-dispersive spectrometer (EDAX, Inc.).

The bound rubber contents were determined by the extraction of the unbound materials, such as the ingredients and free rubbers, with toluene for 3 days and acetone for 1 day followed by drying for 2 days at room temperature until a constant mass value was reached. The toluene was changed every 24 h. The weights of the samples before and after the extraction were measured, and the bound rubber contents were calculated according to the following equation:[14]

$$R_b(\%) = 100 \times [W_{fg} - W_t[m_f/(m_f + m_r)]]/W_t[m_r/(m_f + m_r)] \quad (1)$$

where R_b is the bound rubber content, W_{fg} is the weight of the filler and the gel, W_t is the weight of the sample, m_f is the fraction of filler in the compound, and m_r is the fraction of rubber in the compound.

The flex fatigue properties and dynamic compression properties of all of the vulcanizates were measured according to ISO 132–1999 and ISO 815-1991 with an XP-16 fatigue testing machine (Beijing Huanfeng Chemical Machinery Trial Plant, Beijing, China) and a YS-25 compression fatigue testing machine (Shanghai Chemical Machinery No. 4 Factory, Shanghai, China), respectively. In dynamic compression measurements, the dynamic compression set values were evaluated with the same specimens as used in the heat buildup test. After heat buildup testing, each specimen was left at 25°C for 1 h. Thereafter, its final height (H_f, mm) was measured, and the compression set was calculated with the following equation:

$$\text{Dynamic compression set } (\%) = [(H_0 - H_f)/H_0] \times 100 \quad (2)$$

where H_0 is the original height (mm).

Strain–sweep experiments were performed on a rubber process analyzer RPA 2000 (Alpha Technologies Co., Akron, OH) to measure the dynamic mechanical properties of vulcanizates, that is, the dependences of the storage modulus (G') and loss factor (tan δ) on the shear strain. The experiment was carried out at 60°C with a test frequency of 1 Hz and a strain deformation from 0.28 to 100%.

The rolling loss properties of all of the vulcanizates were measured on a RRS-II rubber rolling loss testing machine (Beijing Wanhuiyifang Science and Technology Development Co., Ltd., Beijing, China) with a loading of 30 kg at room temperature to determine the effects of different filler ratios and the matrix on the material deformation, temperature rise, and power loss. The testing time was 30 min, and the rotational speed was 800 rpm.

Scanning electron microscopy (SEM) micrographs were taken from the flex-fractured surfaces of composites with an S-250-III scanning electron microscope (Cambridge Co., United Kingdom). The objective was to get an insight into the fracture mode in an attempt to draw a picture of the matrix and filler surface. The fractured surfaces of the specimens were vacuum-plated with gold–platinum for electrical conduction before observation.

The micrographs of rubbers were observed by a Hitachi H-800-1 transmission electron microscope (Hitachi Corp., Tokyo, Japan) with an acceleration voltage of 200 kV and a magnification of 5×10^4. The samples were ultramicrotomed at −100°C under liquid nitrogen cooling to give ultrathin sections with a thickness of 70–90 nm and were then placed onto a 200-mesh cooper grid coated with carbon film.

RESULTS AND DISCUSSION

Structural Formation of the N-SSBR/SiO_2/CB Nanocomposites

Star-shaped SSBR was synthesized through random copolymerization with monomers of styrene and butadiene. Then, the

organically modified silica powder was added to the SSBR solution with homogeneous stirring; this was followed by the removal of the solvent and cocoagulation to obtain N-SSBR. Thereafter, the N-SSBR/SiO_2/CB nanocomposite was obtained by mixing with silica/CB and vulcanization. The structural sketch of the preparation process of the N-SSBR/SiO_2/CB nanocomposite is shown in Figure 1.

The final nanocomposite with good dynamic properties was prepared through two steps; these are illustrated in this schematic representation in detail. The first step was the addition of a part of organically modified silica to the SSBR solution and cocoagulation. In this process of solvent removal, the macromolecular chains of rubber gradually got together and simultaneously wrapped these nanosilica particles to form a substantially nanoreinforced composite. These organically modified silica particles had enough space to be dispersed in the matrix, and thus, cocoagulated rubber with a good filler dispersion was obtained. The second step was the mixture of N-SSBR with silica/CB and vulcanization. In this process, the prefilled silica particles occupied some dispersed sites in the N-SSBR matrix; this was beneficial to the repulsion of the subsequently added silica particles to prevent aggregation, and thus, the homogeneous filler dispersion for the N-SSBR/SiO_2/CB nanocomposite was achieved. In this case, the good dispersion of the organically modified silica particles led them to interaction more with macromolecules rather than other particles, and thus, the whole filler–polymer interaction was improved to resist the external cyclic stress well under dynamic conditions.

Structural Characterization of the N-SSBR

After it was extracted by boiling ethanol solvent for 72 h, the N-SSBR sample was tested by ^{1}H-NMR. The ^{1}H-NMR spectrum is shown in Figure 2.

All of the characteristic peaks are exhibited in Figure 2, and there was no signal peak in the chemical shift of 6.20–6.85 ppm. This indicated that the styrene units were randomly distributed rather than block copolymerized. According to the reported equations,[15] the styrene and vinyl (1,2-butadiene structure) contents could be calculated. The molecular weight parameters could also be determined by gel permeation chromatography measurement. In addition, the N-SSBR sample was heated in an aluminum crucible at 600°C for 6 h, and then, the residues were measured by energy-dispersive spectroscopy (EDS) characterization. All of the obtained structural parameters and silicon element contents of SSBR and N-SSBR are listed in Table II.

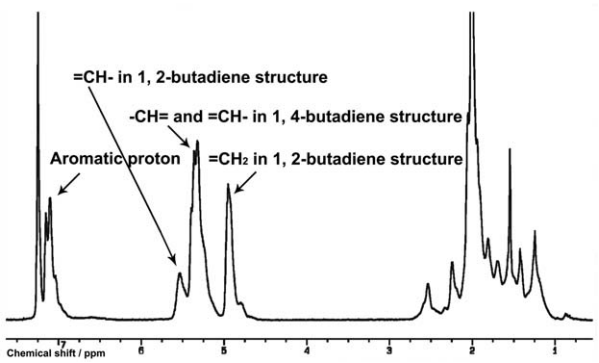

Figure 2. ^{1}H-NMR spectrum of N-SSBR.

The accurate structural information is shown in Table II. The styrene content, vinyl content, and polydispersity index were moderate; this helped to balance the rubber performance. Also, from Figure 2, the Si element content of the residue for the N-SSBR sample was much higher than that for the SSBR sample. The high Si element content of the residue for the N-SSBR sample implied that it could only be derived from the introduction of silica before cocoagulation. In contrast, the low Si element content of the residue for the SSBR sample could only be from impurities. These results confirmed the introduction of silica particles into the matrix for N-SSBR.

Microstructural Characterization

Transmission electron microscopy (TEM) photographs of the microstructures of the N-SSBR cocoagulated rubber and SSBR/SiO_2/CB and N-SSBR/SiO_2/CB nanocomposites are displayed in Figure 3(a,b), respectively.

Generally, in TEM photographs, the light part is the rubber matrix, and the dark part represents the filler particles. As shown clearly in Figure 3(a), the silica particles were dispersed in N-SSBR with a particle size of 30–100 nm and even no aggregation, manifesting as the uniform dispersion of silica in the matrix. There was enough dispersion space for silica to achieve good dispersion in the rubber matrix compared to the rubbers filled with large amounts of silica particles. This showed that cocoagulated rubber with good silica dispersion could be prepared by the cocoagulation method, and it could be a new type of matrix to be filled with other silica particles.

As shown in Figure 3(b), there were obscure hammer-shaped CB particles and spherical-shaped silica particles dispersed in the rubber matrix. It also can be seen that the dispersion of

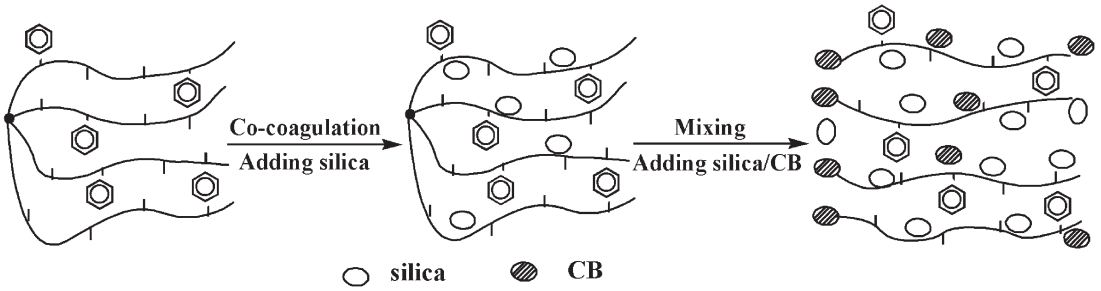

Figure 1. Sketch of the preparation process for the N-SSBR/SiO_2/CB composite.

Table II. Structural Parameters and Silicon Contents of the SSBR and N-SSBR

Rubber	Styrene structure (%)	1,2-Butadiene structure (%)	M_n	M_w	M_w/M_n	Mass fraction of the silicon element displayed in EDS (%)
SSBR	29.5	34.7	35.1×10^4	57.4×10^4	1.63	2.03
N-SSBR	29.5	34.7	35.1×10^4	57.4×10^4	1.63	47.85

silica in N-SSBR was superior to that in SSBR, and this superiority was more significant at high silica/CB ratios. Evident silica networks and large silica agglomerates were observed in the images of the SSBR/SiO_2/CB composite. A possible reason was that the silica particles already dispersed in N-SSBR in the first step hindered the aggregation of silica particles added in the second step; thus, the whole silica dispersion was partly improved. Moreover, N-SSBR with a small amount of silica particles could promote the postfilled silica particles to disperse uniformly in the matrix because of the common compatibility between the silica particles in N-SSBR and those added in the second step.

Filler–Polymer Interaction

The level of bound rubber content was affected by the filler–polymer interaction.[16] The bound rubber contents of the SSBR/SiO_2/CB and N-SSBR/SiO_2/CB–rubber compounds are displayed in Table III.

As shown in Table III, the bound rubber contents of the N series of rubber compounds were correspondingly higher than those of the C series of rubber compounds at the same silica/CB ratio; this indicated stronger interactions between the macromolecular chains and filler particles for the N series of rubber compounds. This demonstrated that the cocoagulation method strengthened the filler–polymer interaction. The results of the TEM observations and bound rubber contents further illustrated that the cocoagulation method was an effective way to improve both the filler dispersion and filler–polymer interaction. This correlation was also reported in some similar studies.[12,17]

The good filler dispersion, together with the strong filler–polymer interactions, for the N series of rubbers contributed to the excellent dynamic properties, which are discussed in detail later.

Dynamic Mechanical Properties

The G'–ε% (where ε% means strain) and tan δ–ε% curves of the SSBR/SiO_2/CB and N-SSBR/SiO_2/CB nanocomposites are shown in Figure 4.

As shown in Figure 4, the G' values of both the C and N series of nanocomposites increased with increasing silica content. This result shows that the affinity of the nonpolar rubber to silica was weaker than that to CB, which contained many nonpolar functional groups, such as quinonyl, phenolic, and inner ester groups, although the silica powder was organically modified by the silane coupling agent. It is well known that silica has strong filler–filler interactions.[18] Therefore, its characteristic of weak filler–rubber interactions became more distinct when a large amount of silica powder was added to the rubber matrix.[19,20]

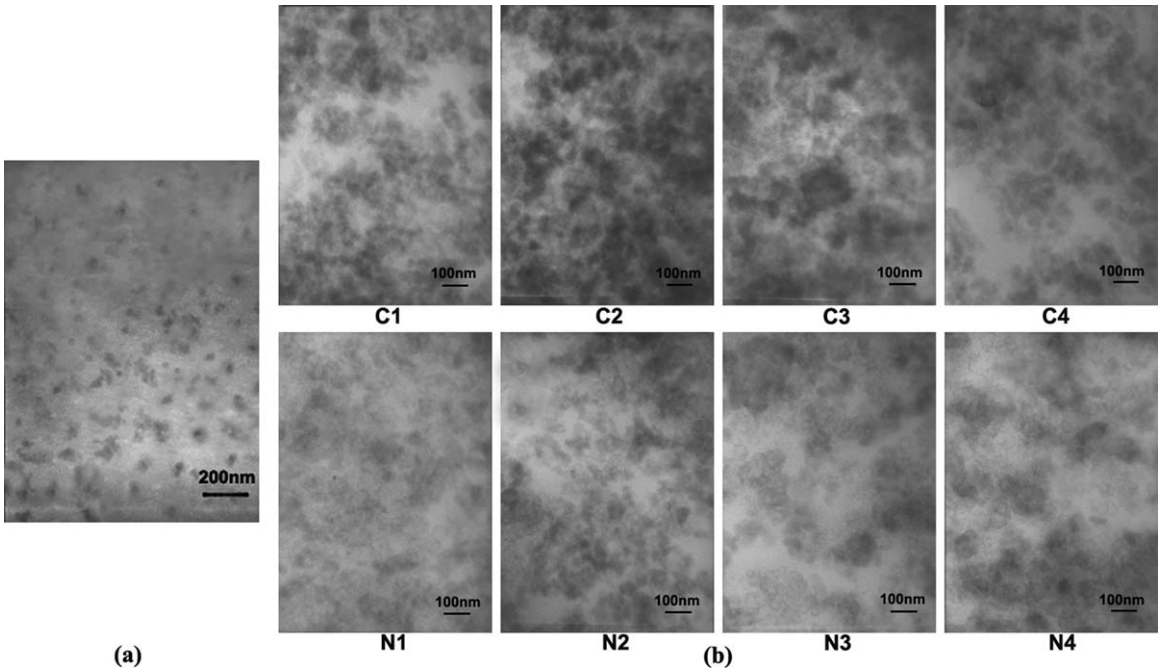

Figure 3. TEM photographs of the (a) N-SSBR and (b) SSBR/SiO_2/CB and N-SSBR/SiO_2/CB nanocomposites.

Table III. Bound Rubber Contents of the Rubber Compounds

	Sample							
	C1	N1	C2	N2	C3	N3	C4	N4
Bound rubber content (%)	33.79	38.58	30.65	33.12	31.48	36.42	29.83	30.54

Lots of silica particles in the rubber matrix were apt to join each other by hydrogen bonding, and thus, aggregate networks were formed. As a result, the viscosity of the composite increased, and thus, an increased G' value was observed. As shown in Figure 4, all of the G' values of the vulcanizates decreased with increasing strain; this was the famous Payne effect.[21] The Payne effect usually depends on the filler content in the rubber compound material and essentially comes from deformation-induced microscopic structural modulation involving the breakage and recovery of weak physical bonds between filler aggregates or clusters. The Payne effect is also directly correlated with the strength of the filler network structure in the rubber matrix.[22] With increasing strain, the filler network in the rubber is more compact, and the decrease in G' value is more pronounced; that is, there is a larger difference in the G' values between the initial and final strain ($\Delta G'$) and a more remarkable Payne effect. The fundamental viewpoints proposed by Ulmer[23] and Huber[24] to understand the Payne effect were that there was always the breakage and recovery of weak physical bonds during deformation. The rate of breakage was assumed to be an increasing function of the strain, and the rate of recovery was assumed to be a decreasing function. Under stationary conditions, which were characterized by a constant strain and stress, there was a dynamic equilibrium between the number of breakage and recovery processes per unit of time.

As shown in Figure 4, the G' values of the N series of nanocomposites were universally lower than those of the C series at the same filler ratios and strains. This result indicated that the N series of nanocomposites had fewer filler network structures; this was consistent with a good filler dispersion for the N-SSBR/SiO_2/CB nanocomposites observed in the TEM images. In the whole strain range, the $\Delta G'$ values for the N series of nanocomposites were lower than those for the C series of nanocomposites, especially at high silica contents; this implied the unnoticeable Payne effect for the N series of nanocomposites.

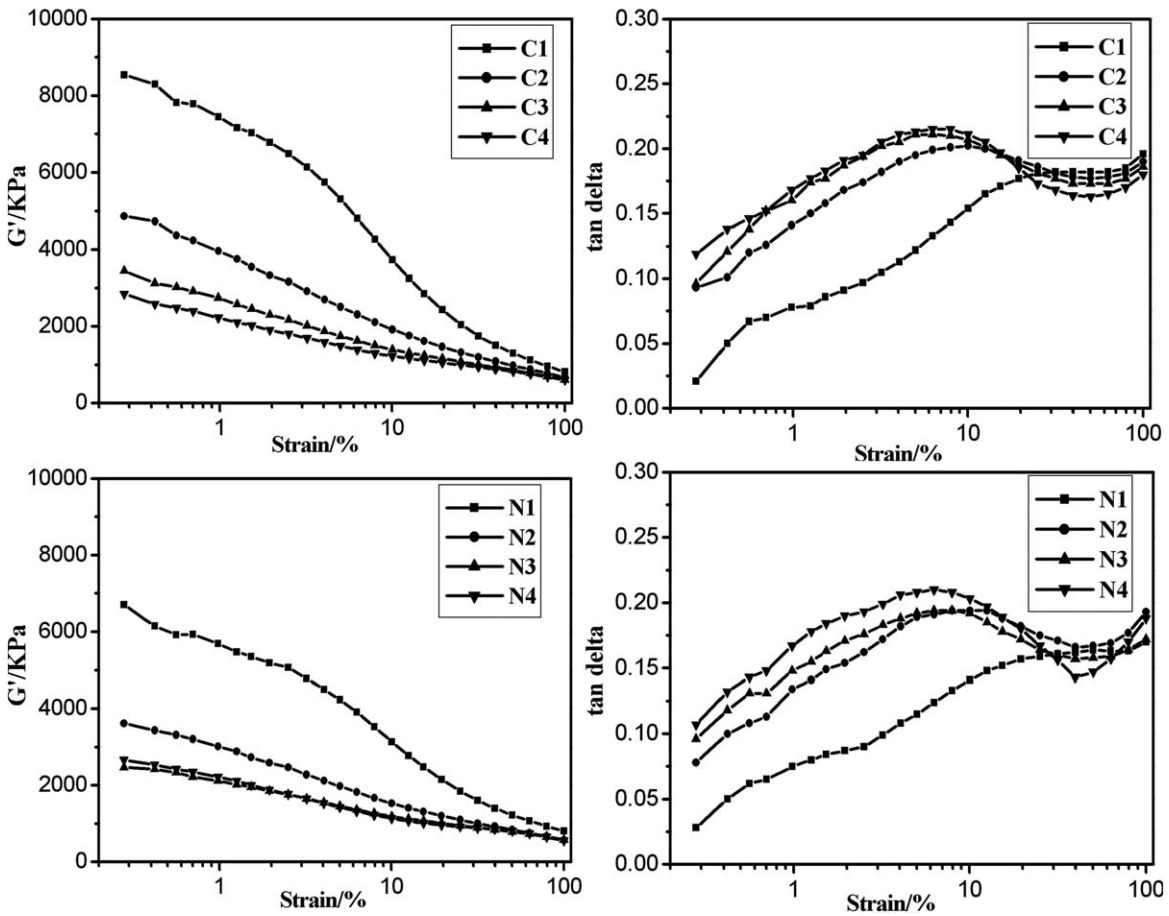

Figure 4. G'–strain and tan δ–strain curves of the SSBR/SiO_2/CB and N-SSBR/SiO_2/CB nanocomposites with different ratios of silica to CB.

The observed phenomena could be discussed with regard to the material microstructure. Because G' is an evaluation of the material stiffness, it is proportional to the number of intact physical bonds, which can transfer forces on the microscopic scale. Its monotonic decline is caused by a decrease in the number of intact bonds with increasing strain.[25] The stronger filler–rubber interfacial interaction and weaker filler network of the N series of nanocomposites led to fewer intact bonds and breakage–recovery processes of weak physical bonds, and thus, the decrease in G' values became smaller with increasing strain. All of the composites exhibited similar G' values when the strain increased to nearly 100%, as the intact bond number caused by the complete destruction of the filler network was approximate. For the C series of nanocomposites, the stronger dependence of G' and shear strain indicated a greater disruption of filler–filler interactions. A large number of silica aggregates and strong filler–filler interactions led to breakage and recovery for lots of weak physical bonds in the filler network during the deformation process; this manifested as a great reduction in the intact bond number with increasing strain.

Comparatively, N-SSBR filled with either 50-phr silica or 20-phr silica/30-phr CB in this study exhibited distinctly lower $\Delta G'$ values and maintained a wider strain range than the N-SSBR filled with 20-phr silica in a previous study.[2] This showed that the cocoagulation method could be beneficial for decreasing the filler network structures and improving filler–polymer interactions, even at a high strain or with doped silica/CB filler, and it could provide advantages for applications in tire tread materials under dynamic conditions.

Tan δ is the ratio of the dissipation modulus (G'') to G', and thus, both tan δ and G'' are used to evaluate the energy loss per loading cycle and are proportional to the breakage rate of bonds. In addition, the breakage rate is proportional to the number of intact bonds, and it increases with increasing strain.[25] From the tan δ–ε% curves in Figure 4, one can see that the changing trends of the tan δ–ε% curves for the two series of nanocomposites were similar. All of the tan δ values increased with an increase in the strain of less than 10%; this was possibly because the macromolecule–macromolecule and macromolecule–filler sliding friction increased with increasing deformation amplitude. In this case, the energy loss increased with increasing strain because there were enough intact bonds. In the strain range between 10 and 40%, because of the instantaneous separation of the filler network from part of the macromolecular chains, all of the tan δ values of the vulcanizates containing CB decreased slightly with increasing strain. This led to a larger decrease in G'' than that in the G' value. In this case, the energy loss decreased with increasing strain because the number of intact bonds decreased considerably. However, the tan δ values of the vulcanizates filled only with silica were apt to be constant when the strain exceeded 30%. This was because these vulcanizates with many filler networks still had a certain amount of intact bonds, and this led to no decrease in the energy loss with increasing strain. In this strain region, the secondary structures of the silica particles were destroyed,[26,27] and the degree of this destruction was in accordance with the decrease in the energy loss produced by filler–macromolecule viscous stress. When the strain exceeded 40%, all of the tan δ values increased again because the heat generated from the microagglomerate destruction caused by intensive friction contributed to the high internal friction loss. In addition, the entrapped rubbers occluded in the microagglomerates were released to enlarge the effective volume of the free molecular chain segments; this led to an increase in the internal friction loss. Compared with the C series of nanocomposites, the N series of nanocomposites all had lower tan δ values, and this indicated that the stronger interfacial interaction, weaker filler network, and lower intact bond number were favorable for decreasing the interfacial slippage and internal friction among the macromolecular chains and reduced the energy loss from the breakage of filler aggregates[28,29] to achieve a decrease in the internal friction heat buildup.

In Figure 4, it also can be seen that in the strain range of less than 20%, all of the tan δ values of the vulcanizates increased with increasing CB content. This indicated that the internal friction of the rubber filled with CB was higher than that of the rubber filled with silica. All of the tan δ values of the vulcanizates containing CB showed maxima at low strain, and these values were higher than those of the vulcanizates only filled with silica because the breakage and recovery of the weak physical bonds of the CB particles needed a large energy loss. These results show that the addition of CB to the rubber matrix was a contributing factor in the internal friction loss.

Comparatively, our test results were similar to those of Wu et al.'s[12] investigation, which used the costly bis[3-(triethoxysilyl) propyl] tetrasulfide as a silane coupling agent. This result provides two advantages: one is the lower cost without effects on the properties, and the other is the significant improvement with N-SSBR as the matrix, which shows broad application prospects for the tire industry.

Flex Fatigue Properties

Figure 5 shows the measurement results of the flex fatigue properties, including the crack generation, crack at 6 degree, and crack propagation rate for both the C and N series of nanocomposites, where the crack at 6 degree indicates that the fatigue crack reached 3 mm.

Compared with the C series of nanocomposites, the N series of nanocomposites exhibited a significantly slower development rate of flex fatigue cracking. This was possibly because the better filler dispersion and stronger interfacial interaction between the silica particles and N-SSBR led to homogeneously distributed bonding between the macromolecular chains and silane chains on the surfaces of the silica particles. Furthermore, these flexible chains of organically modified silica particles were easy to move to homogeneously transfer and distribute the stress over the whole N-SSBR matrix. From the view of energy, the produced energy was gradually accumulated during the process of repeated dynamic deformation and was consumed in the generation and extension of the microcracks. Then, the orientation of microcracks went along the stress direction to separate the filler particles along their edges from the surfaces of the macromolecular chains under a cyclic stress. Consequently, the microcracks were formed by the fracturing of the macromolecular chains. For the N series of nanocomposites, the strong filler–rubber

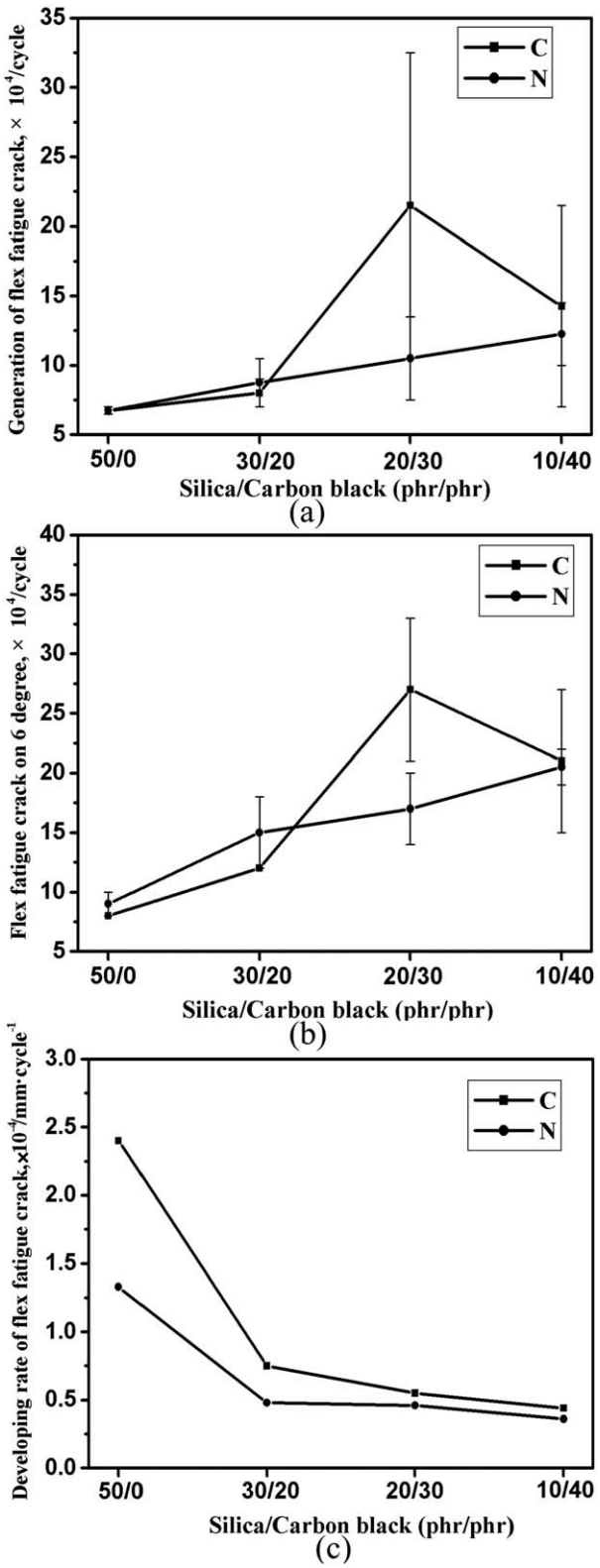

Figure 5. Flex fatigue properties of the SSBR/SiO_2/CB and N-SSBR/SiO_2/CB nanocomposites.

interfacial interaction led to the deformation of macromolecular chains during their energy absorption and energy release and also resisted the external force to consume energy. The caused the stress relaxation to lower the partial external stress and prevent the macromolecular chains from degrading because of the mechanical and chemical damage. As a result, this stress relaxation effectively slowed down the fatigue crack extension. Therefore, the strong ability to resist the repeated deformation for the macromolecular chains of N-SSBR delayed the generation of microcracks and manifested as excellent flex fatigue resistance.

As shown in Figure 5, with decreasing silica/CB ratio, the cycle value of the generating flex fatigue crack increased to a maximum at a silica/CB ratio of 20/30 for the C series of nanocomposites, but it increased continuously for the N series of nanocomposites. The developing rate of crack for both series of nanocomposites decreased. This showed that CB was favorable for resisting the growth of flex fatigue crack. The reason was that after the addition of CB, which had the same polarity with rubber, the produced stress relaxation effectively lowered the cyclic stress and prolonged the pathway of flex crack to resist continuous dynamic deformation well.[30] The good affinity between CB and rubber led to a good matching between the CB and free-volume rubber and to improvements in the load carrying and motion restraint of the macromolecular chains. This indicated excellent resistance to flex fatigue crack extension.

In other literature, there have been few reports on crack generation and development rate; most reports have been on fatigue life. Compared with Lee's[31] investigation, the N4 nanocomposite shown in Figure 5(b) showed more than twice the cycles with only half the CB content. Han and Han[32] reported that it needed 0.5–1.5 $\times$ 10^4 cycles to reach a 3-mm fatigue crack, but the N series of nanocomposites exhibited 8–27 $\times$ 10^4 cycles in this study.

Micromorphologies of the Flex-Fractured Surfaces

In general, the morphologies of fractured surfaces give some information about failure and crack-growth processes. The SEM observations on the flex-fractured surfaces of both the C and N series of the nanocomposites are displayed in Figure 6.

As shown in Figure 6, the fractured surfaces of C1 and C2 exhibited bigger filler particles (some of them were even >2 μm) and more filler aggregates, which easily formed stress concentration points, and thus, some macromolecular chains at the edges of these aggregates were first fractured, and then, clear and bright cracks appeared during dynamic deformation. As a result, the earlier generations of flex fatigue cracks and smoother and straighter crack paths, which mainly extended along a single direction, were observed. On the contrary, for the flex-fractured surfaces of the N1 and N2 nanocomposites, smaller filler particles, obscurer interfaces between the filler and matrix, more tortuous and irregular crack paths, rougher fractured surfaces, and relatively fewer stress concentration points were observed. A rougher fracture surface signified that a higher energy was needed to tear the sample.[33] This result indicates that the use of N-SSBR prepared through the cocoagulation method as the matrix had the remarkable advantages of flex fatigue resistance and flex fatigue crack-growth resistance when the silica content was high. The reason was that the strong interfacial interaction between the filler and rubber[34,35] and the good filler dispersion in the N series of nanocomposites helped to dissipate the accumulative energy produced during the cyclic

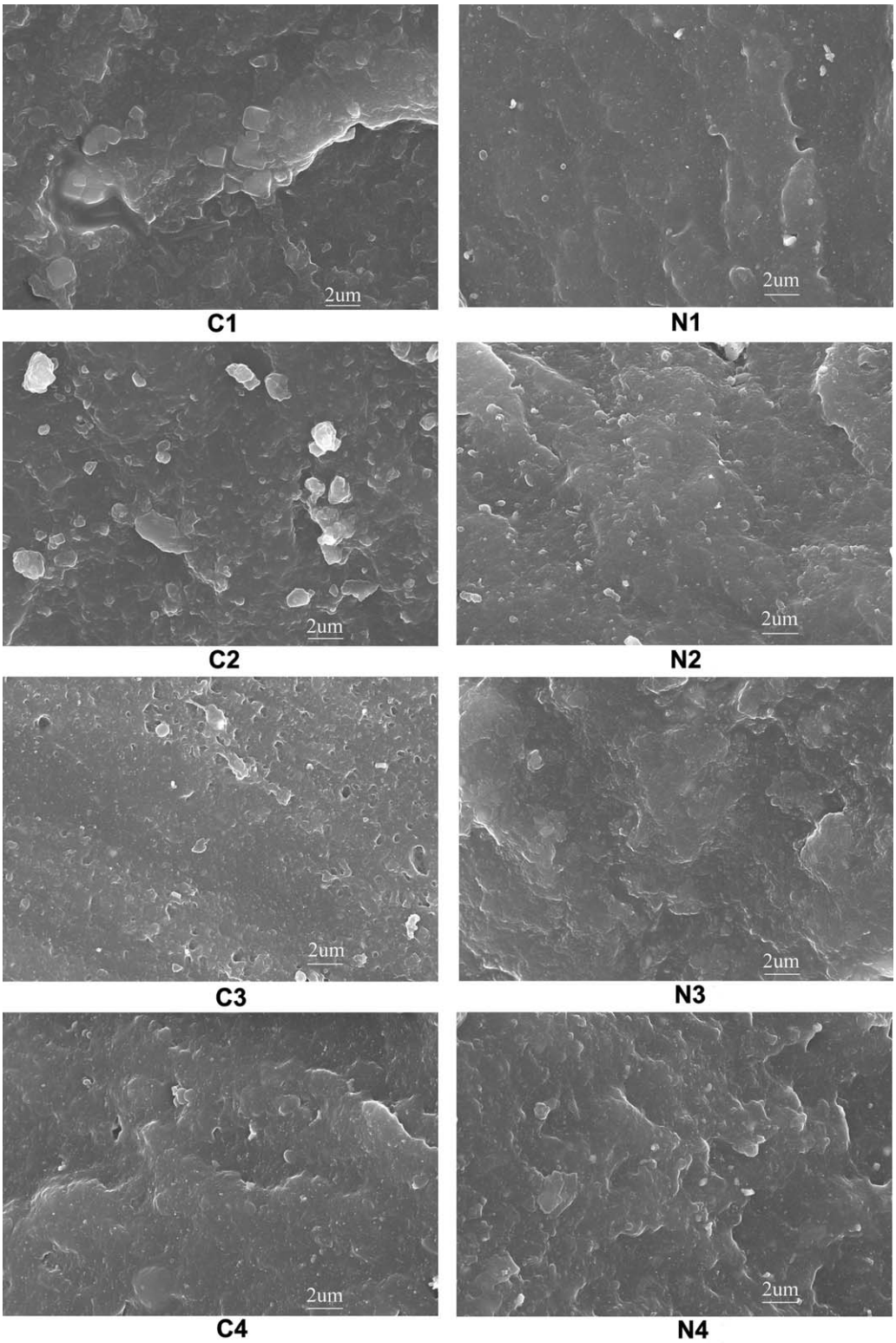

Figure 6. SEM observations of the flex-fractured surfaces of the vulcanizates.

deformation and slow down the growth of the initial cracks. Finally, the initial cracks only extended along the relatively weaker interfaces generated in the process of repeated dynamic deformation. Crack propagation was opposed by the dispersed filler particles in the SSBR matrix, which altered the crack lines, depending on their orientation in the rubber matrix.[36] As a result, the crack extension paths were actually prolonged.

Figure 6 also shows that the cracks on the fractured surfaces of the N3 and N4 nanocomposites were obscure, thick, tortuous,

and branched and manifested as excellent flex fatigue resistance. This implied that the homogeneous stress distribution and tortuous cracks formed at a few weak interfaces could be achieved even at low silica/CB ratio and further demonstrated that the flex fatigue resistance and crack retardation of the vulcanizates could be effectively improved by the cocoagulation method.

Dynamic Compression Properties

Figure 7 shows the dynamic compression properties involving compression heat buildup and compression permanent set for both the C and N series of nanocomposites.

As shown in Figure 7, compared with the C series of nanocomposites, the N series of nanocomposites exhibited lower compression heat buildup and compression permanent set values. The reason for this was that the homogeneous dispersion of silica particles helped to decrease the aggregation and frictional heat with macromolecular chains; in addition, the strong interaction between the filler and rubber matrix reduced the effect of cyclic stress on the deformation of the vulcanizate.[37] When the stress was removed after repeated dynamic compression, the macromolecular chains' elastic recovery for the C series of nanocomposites with poor filler dispersion and weak filler–polymer interaction could not be achieved rapidly; this manifesting as the high compression permanent set values. The results of the low compression heat buildup values for the N series of nanocomposites were in accordance with the low tan δ values displayed in the previous section on the dynamic mechanical properties. Nevertheless, the advantages for the N series of nanocomposites turned out to be inconspicuous with the decreasing silica/CB ratio; this demonstrated that an improvement in the silica dispersion by our cocoagulation technique was easier to realize at high silica contents.

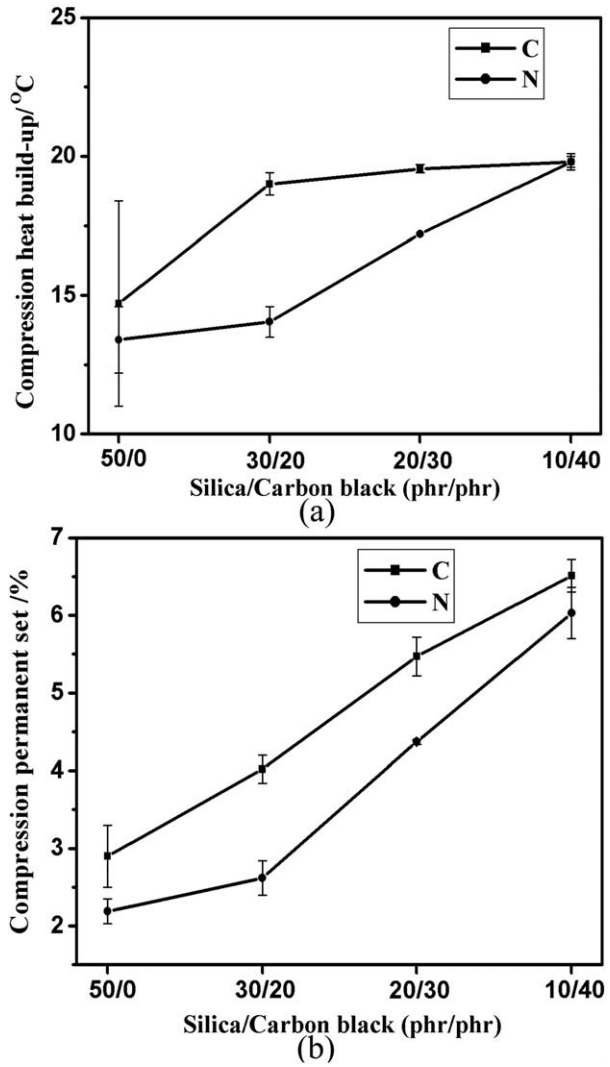

Figure 7. Dynamic compression properties of the SSBR/SiO_2/CB and N-SSBR/SiO_2/CB nanocomposites.

As also shown in Figure 7, the higher the CB content that the nanocomposite contained, the higher the compression heat buildup and compression permanent set values it exhibited. This result also indicates that the slippage–adsorption process on the CB–rubber interfaces and the breakage of the secondary structure of CB generated a high energy consumption of sliding friction on their interfaces during repeated dynamic compression.

There have also been some studies on this. C1 and N1 exhibited lower compression heat buildups (10–15°C) and compression permanent sets (2–3%) than those (18–48°C and 10–35%) reported by Peng et al.[38] A similar superiority was also reflected in a comparison with Kar's report.[39] The compression permanent set of 5.8–6.2% and the compression heat buildups of 62.5–67°C[40] and even 40.8–54.2°C[41] and 85.7–92.3°C[42] were higher than those in our study; this showed the advantage of cocoagulation technique.

Rolling Loss

The measured data of the rolling loss properties for both the C and N series of nanocomposites are shown in Figure 8.

Figure 8 show that the deformation, temperature rise (the increment between the initial and final temperatures), and power loss values for the N series of nanocomposites were all lower than those for the C series of nanocomposites. This result was in accordance with the aforementioned conclusions about other dynamic properties. In Figure 8(a), the result of the lower deformation values for the N series of nanocomposites implies that their good filler dispersion effectively reduced the local stress concentration and resisted deformation. This indicated a low hysteresis characteristic and corresponded to the results of the compression permanent set. For the results represented in Figure 8(b,c), this was possibly because the good filler dispersion and few filler networks for the N series of nanocomposites contributed to lower dynamic heat buildup and hysteresis. In contrast, when each C series of sample periodically rotated under a constant load at a fixed frequency, the relatively weaker filler networks were destroyed because of the deformation forced by the load, and then, the internal friction among the macromolecular chains turned out to be intensive and was followed by the generation of the heat and power loss.

As also shown in Figure 8, the vulcanizate with higher silica contents exhibited relatively lower rolling loss values; this was in accordance with the lower tan δ values measured by rubber

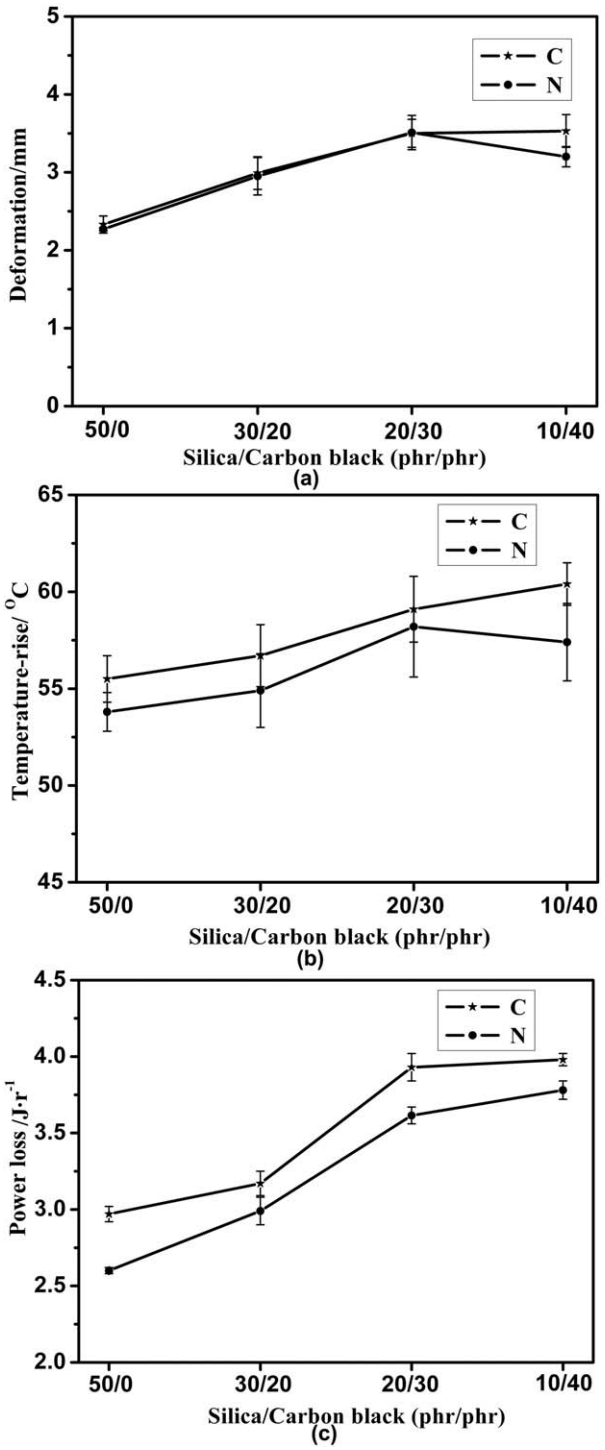

Figure 8. Rolling loss properties of the SSBR/SiO_2/CB and N-SSBR/SiO_2/CB nanocomposites.

process analysis under a certain strain and implied that the addition of silica would be an effective way to lower the rolling resistance of tires.[43] The temperature rise and power loss values of the two series of nanocomposites both basically increased with decreasing silica/CB ratio. The possible reason was the bond dissociation in the interface between the CB and rubber matrix during the sample's experimental process. This indicated that the addition of CB was still a leading factor in the vulcanizate's frictional heat buildup.

There is also literature[44] reporting deformations of 5.45–5.48 mm, temperature rises of 75.3–91.1°C, and power losses of 2.42–2.79 J/r for SSBR filled with silica (50 phr). Comparatively, in our study, N1 nanocomposite exhibited values of 2.27 mm, 53.8°C, and 2.6 J/r, respectively. This comparison represents improvements in the deformation and temperature rise but also the superiority of the cocoagulation technique.

In our previous research,[45] star-shaped SSBR with end groups coupled by $SnCl_4$ had only a small amount of macromolecular chain free ends, so it had a lower internal friction loss than line-shaped SSBR. In this study, the use of N-SSBR prepared by the cocoagulation between silica particles and star-shaped SSBR as a matrix lowered the hysteresis and heat buildup of the composite further.

In summary, for the application in tire tread materials, it is important for the prepared composites to exhibit excellent performance under the dynamic conditions. All of the previous results show that nanocomposites with excellent performance were acquired by the cocoagulation method. Depending on the characteristics of improving filler dispersion and interfacial interaction, N-SSBR could be used as an ideal tread material for preparing high-performance tires. After they were filled with silica and CB at a constant content of 50 phr total, the dynamic properties of the prepared composites in this study were quantitatively compared with those of SSBR composites reported by other researchers, and ours showed significantly better dynamic properties. Thus, the N-SSBR/SiO_2/CB nanocomposites showed great advantages for applications in tire tread materials.

CONCLUSIONS

1. N-SSBR was prepared through the cocoagulation method, and its structural characterizations showed a homogeneous filler dispersion. This was beneficial to the improvement of the dispersions of the postfilled fillers.
2. The N-SSBR/SiO_2/CB–rubber compounds exhibited higher bound rubber contents. This result implies strong filler–polymer interactions, which, together with good filler dispersion, were the main causes of the improvements in the dynamic properties.
3. The N-SSBR/SiO_2/CB nanocomposites exhibited lower G' values, Payne effects, internal friction loss, compression heat buildup, compression permanent set, and rolling power loss, and these advantages become more prominent at high silica/CB ratios.
4. The N-SSBR/SiO_2/CB nanocomposites exhibited better flex fatigue resistance, and they also showed good abilities to disperse stress and resist crack propagation. This was manifested as rough and tortuous cracks on the fractured surfaces of the flex fatigue sections.
5. The cocoagulation method for the preparation of a rubber matrix with good filler dispersion is an effective technique for improving the dynamic properties. N-SSBR used as a polymer matrix, therefore, is one kind of high-performance material that could be applied to green tire tread.

ACKNOWLEDGMENTS

The authors gratefully acknowledge the financial support of the National Tenth Five-Year Plan (contract grant number 2004BA310A41), the National Natural Science Foundation of China (contract grant numbers 50573005 and 51208012), and the Research Fund of New Teachers for the Doctoral Program of Higher Education of China (contract grant number 3c009011201301).

REFERENCES

1. Bertora, A.; Castellano, M.; Marsano, E.; Alessi, M.; Conzatti, L.; Stagnaro, P.; Colucci, G.; Priola, A.; Turturro, A. *Macromol. Mater. Eng.* **2011**, *296*, 455.
2. Liu, X.; Zhao, S. H. *J. Appl. Polym. Sci.* **2008**, *109*, 3900.
3. Movahed, S. O.; Ansarifar, A.; Song, M. *Polym. Int.* **2009**, *58*, 209.
4. Shin, C. H.; Kim, D. S. *Polym. Adv. Technol.* **2008**, *19*, 1062.
5. Sae-Oui, P.; Sirisinha, C.; Thepsuwan, U.; Hatthapanit, K. *Polym. Test.* **2004**, *23*, 871.
6. Mohanty, T. R.; Bhandari, V.; Chandra, A. K.; Chattopadhyay, P. K.; Chattopadhyay, S. *Polym. Compos.* **2003**, *34*, 214.
7. Bhadra, S.; De, P. P.; Mondal, N.; Mukhapadhyaya, R.; Gupta, S. D. *J. Appl. Polym. Sci.* **2003**, *89*, 465.
8. Ghosh, A. K.; Maiti, S.; Adhikari, B.; Ray, G. S.; Mustafi, S. K. *J. Appl. Polym. Sci.* **1997**, *66*, 683.
9. Choi, S. S. *J. Appl. Polym. Sci.* **2006**, *99*, 691.
10. Yan, H. X.; Sun, K.; Zhang, Y.; Zhang, Y. X.; Fan, Y. Z. *J. Appl. Polym. Sci.* **2004**, *94*, 1511.
11. Liu, X.; Zhao, S. H.; Yang, Y.; Zhang, X. Y.; Wu, Y. P. *Polym. Adv. Technol.* **2009**, *20*, 818.
12. Wu, Y. P.; Zhao, Q. S.; Zhao, S. H.; Zhang, L. Q. *J. Appl. Polym. Sci.* **2008**, *108*, 112.
13. Sun, J.; Song, Y. H.; Zheng, Q.; Tan, H.; Yu, J.; Li, H. *J. Polym. Sci. Part B: Polym. Phys.* **2007**, *45*, 2594.
14. Choi, S. S.; Kim, I. S. *Eur. Polym. J.* **2002**, *38*, 1265.
15. Feng, H. D.; Zhang, X. Y.; Zhao, S. H. *J. Appl. Polym. Sci.* **2008**, *110*, 228.
16. Mohsen, M.; Abdel-El Salam, M. H.; Ashry, A.; Ismail, A.; Ismail, H. *Polym. Degrad. Stab.* **2005**, *87*, 381.
17. Mélé, P.; Marceau, S.; Brown, D.; De Puydt, Y.; Albérola, N. D. *Polymer* **2002**, *43*, 5577.
18. Evans, L. R.; Fultz, W. C. *Rubber World* **1998**, *219*, 38.
19. Donnet, J. B. *Rubber Chem. Technol.* **1998**, *71*, 323.
20. Fröhlich, J.; Niedermeier, W.; Luginsland, H. D. *Composites* **2005**, *36*, 449.
21. Payne, A. R. In Reinforcement of Elastomers; Kraus, G., Ed.; Interscience: New York, **1965**; Chapter 3.
22. Wang, M. *J. Rubber Chem. Technol.* **1999**, *72*, 430.
23. Ulmer, J. D. *Rubber Chem. Technol.* **1996**, *69*, 15.
24. Huber, G. *Doctoral Thesis, University of Mainz*, **1997**.
25. Lion, A.; Kardelky, C. *Int. J. Plast.* **2004**, *20*, 1313.
26. Payne, A. R. *J. Appl. Polym. Sci.* **1962**, *6*, 57.
27. Payne, A. R.; Whittaker, R. E. *Rubber Chem. Technol.* **1971**, *44*, 440.
28. Cassagnau, P.; Mélis, F. *Polymer* **2003**, *44*, 6607.
29. Cassagnau, P. *Polymer* **2003**, *44*, 2455.
30. Ismail, H.; Anuar, H. *Polym. Test.* **2000**, *19*, 349.
31. Lee, B. L. *Polym. Eng. Sci.* **1982**, *22*, 902.
32. Han, S. C.; Han, M. H. *J. Appl. Polym. Sci.* **2002**, *85*, 2491.
33. Teh, P. L.; Ishak, Z. A. M.; Hashim, A. S.; Karger-Kocsis, J.; Ishiaku, U. S. *Eur. Polym. J.* **2004**, *40*, 2513.
34. Wang, J.; Jia, H.; Ding, L.; Zhu, L.; Dai, X.; Fei, X.; Li, F.; Gong, X. *Polym. Compos.* **2013**, *34*, 690.
35. Sui, G.; Zhong, W. H.; Yang, X. P.; Yu, Y. H.; Zhao, S. H. *Polym. Adv. Technol.* **2008**, *19*, 1543.
36. Malas, A.; Das, C. K. *Polym. Eng. Sci.* **2014**, *54*, 33.
37. Rattanasom, N.; Saowapark, T.; Deeprasertkul, C. *Polym. Test.* **2007**, *26*, 369.
38. Peng, H.; Liu, L.; Luo, Y.; Hong, H.; Jia, D. *J. Appl. Polym. Sci.* **2009**, *112*, 1967.
39. Kar, K. K.; Bhowmick, A. K. *J. Appl. Polym. Sci.* **1997**, *64*, 1541.
40. Ostad-Movahed, S.; Ansarifar, A.; Song, M. *J. Appl. Polym. Sci.* **2009**, *113*, 1868.
41. Choi, S. S.; Chung, K. H.; Nah, C. *Polym. Adv. Technol.* **2003**, *14*, 557.
42. Saeed, F.; Ansarifar, A.; Ellis, R. J.; Haile-Meskel, Y.; Irfan, M. S. *J. Appl. Polym. Sci.* **2012**, *123*, 1518.
43. Wolff, S.; Wang, M. J.; Tan, E. H. *Kautsch. Gummi Kunstst.* **1995**, *48*, 82.
44. Xu, C. Y.; Wu, Y. P.; Zhao, S. H.; Zhang, X. Y. *China Synth. Rubber Ind.* **2009**, *32*, 201.
45. Zhao, S. H.; Zhang, X. Y.; Jin, G. T. *China Elast.* **1995**, *5*, 25.